A Method for the Design of Shock-Free Slender Bodies of Revolution

A. A. Hassan*
Arizona State University, Tempe, Arizona

A numerical procedure is presented for the design of shock-free supercritical slender bodies of revolution. The procedure relies on the fact that for small disturbances a hodograph-like transformation (not known a priori) can be applied to the axisymmetric potential equation. This results in a set of two coupled Poisson equations defined on a common rectangular domain. With the special variables used, the system of coupled equations for the subsonic portion of the flow is solved iteratively using a fast Poisson solver. This in turn, defines the mapping of the subsonic or subsonic-sonic boundary in the physical plane. For supercritical flows, the supersonic portion of the flow is calculated from data on the sonic line using an axisymmetric characteristic calculation. This is followed by a map to the physical plane to determine the shape of the body under the sonic bubble. Examples of shock-free supercritical slender body designs are presented and show good agreement with the direct computation of the flow past the designed slender bodies.

Introduction

In the last decade there has been much interest in the transonic flight regime. In particular, axisymmetric transonic flow is of interest not only because of its practical application to missile and launch vehicle aerodynamics, but also because knowledge of the aerodynamic properties of a body of revolution in axisymmetric flow, when considered with the area rule of Hayes,[1] Whitcomb,[2] and/or the equivalence rule of Oswatitsch and Keune[3] permits the calculation of the aerodynamic properties of such bodies. This equivalence, clearly stated by Lomax,[4] permits the ready calculation of the linear drag, and in supersonic flow the linear lift of wings, bodies, and wing-body combinations as the overall aerodynamic characteristics only depend on the cross section area of the equivalent body of revolution.

Mathematically, the direct or analysis, and the design or inverse problems of slender bodies of revolution are treated as two distinct problems. In the former, a slender body is chosen and its aerodynamic characteristics such as lift, drag, and moment coefficients are determined. In the latter, a body geometry is sought which supports a preassigned target velocity or pressure distribution. A typical implementation is to smooth out discontinuities in the surface pressure distribution that would be associated with shocks. In principle, this process could lead to a reduction in wave drag. Moreover, it is well known that many desirable requirements for the flow of air past a solid surface, e.g., delay of laminar-turbulent transition or separation of the boundary layer, may be met by imposing certain conditions on the velocity distribution along the surface.[5,6] The ability to design slender-body shapes that will provide a given pressure distribution is, therefore, highly desirable.

While major progress has been made in the analysis of transonic slender bodies of revolution by Keune and Oswatitsch,[7] Kusukawa,[8] Spreiter and Alksne,[9,10] Krupp and Murman,[11] Sedin,[12] and many others, similar efforts for the inverse problem have been lacking. Zannetti[13] has reported a time-dependent procedure to solve the inverse problem for internal axisymmetric flows. In his method, based on iterated solutions of the direct problem, he solves the time-dependent Euler's equations utilizing a predictor-corrector difference scheme suggested by McCormack. A similar design procedure had also been developed earlier by Nelson et al.[14] In the method of Shankar,[15] shocked as well as shock-free slender-body designs were obtained through iterative solutions of the transonic small disturbance potential equation. The prescribed pressure distribution on the unknown surface of the body was implemented numerically: once as a Neumann boundary condition, and in a different procedure as a Dirichlet boundary condition. It was concluded that the Dirichlet boundary condition approach was more robust and always yielded converging results sooner than the Neumann approach.

Following the recent success of the two-dimensional transonic airfoil design methos using numerical optimization techniques (Hicks and Vanderplaats,[16] and Hicks and Henne[17]), a design procedure for axisymmetric bodies of minimum wave drag was developed by Chan and Mundie.[18] In their method, direct solutions are sought with a slender body shape that is numerically optimized to yield bodies of minimum wave drag. A complete account of this theory can be found in Miele.[19] Recently, Malmuth et al.[20] described an optimization procedure for the design of transonic lifting wing-body combinations. In their procedure the body shape is expressed in terms of a finite number of parameters. The optimization problem for some aerodynamic quantity such as drag, as a function of these parameters, was then solved using decision theory.

The numerical procedure developed here[21] for the design of shock-free slender bodies of revolution is based on the solution of the small disturbance potential equation. Instead of using a mixed-difference scheme to account for the embedded supersonic flow region, we have temporarily decoupled the subsonic and supersonic flow regions.

In this paper, we first discuss the small disturbance flow equations and their transformation to the computational plane where they are quasilinear. We then demonstrate, through examples, the accuracy of the design method by comparing our results with those obtained from a direct computation of the flow past the designed slender body using a mixed finite-difference scheme, RAXBOD.[22]

Basic Equations

The mathematic formulation of the problem assumes a steady, axisymmetric, irrotational flow of a perfect gas. The

Received Nov. 30, 1983; revision received Aug. 19, 1985.

*Assistant Professor, Mechanical and Aerospace Engineering Department. Member AIAA.

small disturbance equation governing the perturbation potential ϕ, is

$$(\gamma+1)\left(\frac{\partial\phi}{\partial x}\right)\left(\frac{\partial^2\phi}{\partial x^2}\right)-\frac{a^*}{r}\frac{\partial}{\partial r}\left(r\frac{\partial\phi}{\partial r}\right)=0 \tag{1}$$

Here, x and r are normalized cylindrical space coordinates, x being directed along the axis of symmetry of the body and r normal to the axis of symmetry. The local sound velocity a^* is defined through the energy equation and γ is the ratio of specific heats. Equation (1) is elliptic when $(\partial\phi/\partial x)<0$ (subsonic flow), hyperbolic when $(\partial\phi/\partial x)>0$ (supersonic flow), and parabolic where $(\partial\phi/\partial x)=0$ (sonic flow). To solve Eq. (1) two boundary conditions must be provided: 1) the behavior of the flow in the far field, and 2) the flow tangency condition on the slender body surface. In the inverse-design procedure presented here, the pressure distribution (or equivalently the velocity) is used as input rather than the body coordinates. Accordingly, for the inverse problem, a Neumann boundary condition for ϕ on the surface of the body cannot be prescribed since its location is unknown a priori.

Utilizing the definitions of the perturbation velocities $\bar{u}$ and $\bar{v}$, viz.,

$$\frac{\partial\Phi}{\partial x}=a^*+(1-M_\infty)\frac{\partial\phi}{\partial x}=a^*+\bar{u}$$

$$\frac{\partial\Phi}{\partial r}=(1-M_\infty)\frac{\partial\phi}{\partial r}=\bar{v} \tag{2}$$

we express Eq. (1) as

$$(\gamma+1)\bar{u}\frac{\partial\bar{u}}{\partial x}-\frac{a^*}{r}\frac{\partial}{\partial r}(r\bar{v})=0 \tag{3}$$

In addition, eliminating ϕ from Eqs. (2) through cross differentiation, we obtain

$$\frac{\partial\bar{u}}{\partial r}-\frac{\partial\bar{v}}{\partial x}=0 \tag{4}$$

Equations (3) and (4) are the system of equations to be solved in the computational plane. The coordinate transformation is described in the following section.

Transformed Equations

Introducing the new set of variables X, Y, U, and V defined by the equations

$$x=X \tag{5a}$$

$$r=\lambda Y \tag{5b}$$

$$\bar{u}=\pm 1.5\lambda a^* U^{2/3} \tag{5c}$$

$$\bar{v}=\lambda a^* V/r \tag{5d}$$

and reformulating the partial derivatives in Eqs. (3) and (4) in terms of the new variables, we obtain

$$\frac{\partial V}{\partial Y}-YU^{1/3}\frac{\partial U}{\partial X}=0 \tag{6a}$$

$$\frac{\partial V}{\partial X}\pm YU^{-1/3}\frac{\partial U}{\partial Y}=0 \tag{6b}$$

In Eqs. (5c) and (6b) $\pm$ refers to subsonic and supersonic flow conditions respectively, and λ is a constant defined by

$$\lambda=[1.5(\gamma+1)]^{-1/3} \tag{6c}$$

Referring to Fig. 1, we consider the transformation function given by the solution of the coupled system of partial differential equations:

$$\frac{\partial X}{\partial s}-U^{1/3}\frac{\partial Y}{\partial t}=0 \tag{7a}$$

$$\frac{\partial X}{\partial t}\pm U^{1/3}\frac{\partial Y}{\partial s}=0 \tag{7b}$$

Equations (7) indicate that the mapping from the physical x-r plane to the computational s-t plane is solution-dependent and therefore, unknown prior to the solution procedure. Moreover, in regions of subsonic flow the mapping is governed by an elliptic partial differential equation, and in regions of supersonic flow it is governed by a hyperbolic partial differential equation.

Reformulating the definitions for the partial derivatives in Eqs. (6a) and (6b) in terms of s and t, we obtain the system of equations

$$\frac{\partial V}{\partial t}-Y\frac{\partial U}{\partial s}=0 \tag{8a}$$

$$\frac{\partial V}{\partial s}\pm Y\frac{\partial U}{\partial t}=0 \tag{8b}$$

Equations (8) are the s-t plane counterpart of the physical plane equations [Eqs. (3) and (4)]. Elimination of X from Eqs. (7) and V from Eqs. (8) through cross differentiation yields a coupled system of Poisson equations involving U and Y, viz.,

$$\frac{\partial^2 U}{\partial s^2}\pm\frac{\partial^2 U}{\partial t^2}=-\left(\frac{(\partial Y/\partial s)}{Y}\frac{\partial U}{\partial s}\pm\frac{(\partial Y/\partial t)}{Y}\frac{\partial U}{\partial t}\right) \tag{9a}$$

$$\frac{\partial^2 Y}{\partial s^2}\pm\frac{\partial^2 Y}{\partial t^2}=-\frac{1}{3}\left(\frac{(\partial Y/\partial s)}{U}\frac{\partial Y}{\partial s}\pm\frac{(\partial U/\partial t)}{U}\frac{\partial Y}{\partial t}\right) \tag{9b}$$

It is noteworthy that the numerical transformation given by Eqs. (7) to the computational plane results in a coupled system of quasilinear second-order-partial differential equations for U and Y. This was first pointed out by Sobieczky.[21] In addition to this linearity, the major advantages of this transformation are the representation of the physical subsonic-sonic boundary by a rectangular domain (see Fig. 1), and the decoupling of the subsonic and supersonic regions of the flowfield.

Subsonic Flow Region

We proceed by considering the subsonic region, abcdefgh, of the flowfield depicted in Fig. 1. The governing equations for U and Y in the computational plane are

$$\frac{\partial^2 U}{\partial s^2}+\frac{\partial^2 U}{\partial t^2}=-\left(\frac{(\partial Y/\partial s)}{Y}\frac{\partial U}{\partial s}+\frac{(\partial Y/\partial t)}{Y}\frac{\partial U}{\partial t}\right) \tag{10a}$$

$$\frac{\partial^2 Y}{\partial s^2}+\frac{\partial^2 Y}{\partial t^2}=-\frac{1}{3}\left(\frac{(\partial U/\partial s)}{U}\frac{\partial Y}{\partial s}+\frac{(\partial U/\partial t)}{U}\frac{\partial Y}{\partial t}\right) \tag{10b}$$

To complete the boundary value problems for U and Y, appropriate boundary conditions must be prescribed in the s-t plane on the common rectangle ($0\le s\le 1$, $0\le t\le 1$). The system of horizontal grid lines utilized in the s-t plane is one which conforms to the shape of the subsonic portion of the body and its sonic line when transformed back to the physical x-r plane. Therefore, the boundary conditions prescribed along $t=0$ represent conditions on the actual un-

mapped (or unstretched) subsonic portion of the body and its sonic line. The numerical boundary conditions described subsequently were found to be most consistent with the physics of the flow problem.

1) Far field, boundary ga. The perturbation quantity $U(s,1)$ maintains a constant, but small value B_1

$$U(s,1)=B_1 \tag{11}$$

Therefore, along boundary ga, $\partial U(s,1)/\partial s \approx 0$, and $\partial U(s,1)/\partial t \approx 0$. Equation (10b) then reduces to

$$\frac{\partial^2 Y(s,1)}{\partial s^2}+\frac{\partial^2 Y(s,1)}{\partial t^2}\cong 0 \tag{12}$$

Considering only the first harmonic of the solution to the above equation, we obtain

$$Y(s,1)=B_2\sin(\pi s) \tag{13}$$

2) Boundaries ab and gf. For symmetrical slender-body designs at zero incidence, like those considered in the present study, identical boundary conditions are prescribed along ab and gf, viz.,

$$U(0,t)=-K\exp\left(\frac{-1}{t-1}\right)+B_1 \quad 0\le t\le 1$$

$$=U(1,t) \tag{14}$$

In Eq. (14) K assumes the value of 1 for slender-body designs having cusped leading and trailing edges (points b and f, respectively) and a value of $1/t$ for slender-body designs having sharp leading and trailing edges. This behavior is found to be consistent with the well known results obtained from the small disturbance theory (Ashley and Landahl[23]). Referring to Fig. 1 and Eq. (5b), one finds

$$Y(0,t)=Y(1,t)=0 \quad 0\le t\le 1$$

It should be observed, that if the boundary value problems for $V(s,t)$ and $X(s,t)$ were to be solved instead of those for $U(s,t)$ and $Y(s,t)$, then the commonly utilized boundary condition $V(0,t)=0$ would have been used along ab, gf. Indeed, the task of prescribing $X(0,t)$ would have been more difficult compared to prescribing $Y(0,t)=0$. Moreover, the consistency of the boundary condition $Y(0,t)=0$ with $V(0,t)=0$ in the present formulation is clear from Eqs. (5b) and (5d).

As for the boundary condition $U(0,t)$, it is of utmost importance to bear in mind that this distribution is not retained upon carrying the map to the physical plane. Nonetheless, a stretched (or distorted) form of this distribution is the final outcome (e.g., one may find a nonlinear transformation which transforms a sine function in one coordinate system to a parabolic function in a second coordinate system). Here, the amount of nonlinear stretching is given by the numerical integration of Eqs. (7). It is perhaps clearer if we visualize the entire subsonic-sonic boundary (Fig. 1) stretching in accordance with the solution of Eqs. (7) to accommodate the prescribed U distribution along the four boundaries. Equations (8), which represent the governing equations in the computational plane are, therefore, indirectly satisfied since Eqs. (9) are only reduced forms of Eqs. (7) and (8). It should also be observed that numerical integration of Eqs. (8) along $s=0$, $s=1$ guarantees that $V(0,t)=V(1,t)=0$ irrespective of the $U(0,t)$, $U(1,t)$ distributions prescribed.

3) Subsonic-sonic boundary bcdef. For supercritical flows as those discussed here we have along bc ($s<s_c$) and along ef ($s>s_e$)

$$U(s,0)=A_2(s)-A_1\log(s(1-s)), \quad Y(s,0)=g_1(s) \tag{15}$$

and along the sonic line cde

$$U(s,0)=0, \quad Y(s,0)=g_2(s) \quad s_c\le s\le s_e \tag{16}$$

In Eq. (15), A_1 is a positive constant which has a value of zero for cusped leading and trailing edge designs and has other values, as will be discussed later, for sharp leading and trailing edge designs. In Eqs. (11) and (13), B_1 and B_2 are input constants for the design procedure. The functions $g_1(s)$, $g_2(s)$, and $A_2(s)$ are input arbitrary continuous functions representing the radial coordinates of the unstretched body, sonic line radial coordinates (in the sense that knowledge of the x coordinate determines the amount by which the r coordinates are stretched), and the subsonic perturbation velocity distribution necessary for the design procedure, respectively.

The boundary value problems for U and Y are now complete and Eqs. (10) are then solved iteratively using a second-order-accurate fast Poisson solver devised by Sweet.[24] The results for the gradient ($\partial Y/\partial t$) along the elliptic boundary, consisting of the subsonic portion of the slender body and the sonic line, are then utilized to find the inverse map (or

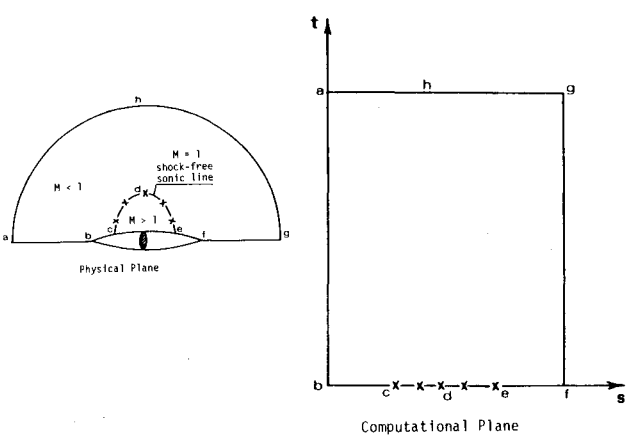

Fig. 1 Sketch of shock-free flow past a slender body of revolution in the physical plane and its corresponding computational s-t plane.

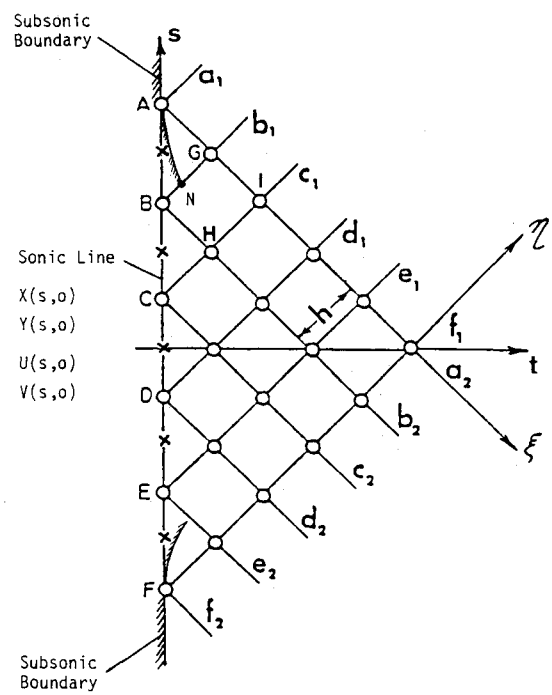

Fig. 2 Computation of the supersonic flowfield in the computational plane (s-t) using the method of characteristics.

the amount of stretching) to the physical plane. That is, numerically integrating Eq. (7a) along the elliptic boundary, viz.,

$$X(s) = \int_{s_b}^{s_f} U^{1/3}(s,0)\frac{\partial Y(s,0)}{\partial t}\,ds \tag{17}$$

we obtain the stretching function $X(s)$. This, in conjunction with Eq. (5b), determines the physical plane shape of the subsonic-sonic boundary bcdef. In this design procedure, numerical integration of Eq. (8b), viz.,

$$V(s,0) = \int_{s_a}^{s_g} Y(s,0)\frac{\partial U(s,0)}{at}\,ds \tag{18}$$

is needed to determine V on the elliptic boundary, abcdefg. Results obtained from the solution of the subsonic flow equations (10) for U and Y, and from Eqs. (17) and (18) for X and V on the sonic line, are then used as initial data for solving the supersonic flow equations [Eqs. (9)]. This is accomplished by using the method of characteristics as explained below.

Supersonic Flow Region

It follows from Eqs. (18) for the flow in the embedded supersonic region, where $U>0$, that both U and Y satisfy the linear wave equations

$$\frac{\partial^2 U}{\partial s^2} - \frac{\partial^2 U}{\partial t^2} = -\left(\frac{(\partial Y/\partial s)}{Y}\frac{\partial U}{\partial s} - \frac{(\partial Y/\partial t)}{Y}\frac{\partial U}{\partial t}\right) \tag{19a}$$

$$\frac{\partial^2 Y}{\partial s^2} - \frac{\partial^2 Y}{\partial t^2} = -\frac{1}{3}\left(\frac{(\partial U/\partial s)}{U}\frac{\partial Y}{\partial s} - \frac{(\partial U/\partial t)}{U}\frac{\partial Y}{\partial t}\right) \tag{19b}$$

which have characteristics of the form

$$ds/dt = \pm 1$$

Introducing the characteristic coordinates ξ,η defined by $\xi = s+t$ and $\eta = s-t$, and reformulating the partial derivatives in Eqs. (7) and (8) in terms of the new coordinates, we obtain

$$\frac{\partial X}{\partial \xi} - U^{1/3}\frac{\partial Y}{\partial \xi} = 0, \qquad \frac{\partial X}{\partial \eta} + U^{1/3}\frac{\partial Y}{\partial \eta} = 0 \tag{20}$$

$$\frac{\partial V}{\partial \xi} - Y\frac{\partial U}{\partial \xi} = 0, \qquad \frac{\partial V}{\partial \eta} + Y\frac{\partial U}{\partial \eta} = 0 \tag{21}$$

Equations (20) and (21) may also be expressed on $\eta =$ constant as

$$dX - U^{1/3}dY = 0 \tag{22a}$$

$$dV - YdU = 0 \tag{22b}$$

and on $\xi =$ constant as

$$dX + U^{1/3}dY = 0 \tag{23a}$$

$$dV + YdU = 0 \tag{23b}$$

With $U(s,0)$ and $V(s,0)$ known on the sonic line having coordinates $X(s,0)$, and $Y(s,0)$, we proceed to solve the two sets of compatibility equations [Eqs. (22) and (23)], holding along the two families of characteristics using a step-by-step numerical scheme (Massau finite-difference scheme). The basic concept of this scheme is the following:

Through each point A,B,C,D,E,F, of the sonic line, line AF in Fig. 2, two characteristics pass, one of the first family, $\eta =$ constant (a_1, b_1, c_1,..., f_1), and one of the second family, $\xi =$ constant (a_2, b_2, c_2,..., f_2). Since the coordinates s and t at the points of the line AF are known, the constants of Eqs. (22) and (23) for each characteristic line a_1,... f_1, a_2,... f_2, at each point of AF, are also known. Consequently, Eqs. (22a) and (23a) applied along two characteristics of opposite families, e.g., b_1 and a_2 of Fig. 2, give two equations relating X_G, Y_G, and U. These can be solved to obtain X and Y at point G as functions of X, Y, and U at the points A and B, viz.,

$$X_G = 0.5(X_A + X_B) + 0.5U^{1/3}(Y_A - Y_B)$$

$$Y_G = 0.5(Y_A + Y_B) + 0.5U^{-1/3}(X_A - X_B) \tag{24}$$

In Eqs. (24), U may be approximated by average values, i.e.,

$$\text{along AG} \qquad U(\xi,\eta) = 0.5(U_A + U_G)$$

$$\text{along BG} \qquad U(\xi,\eta) = 0.5(U_B + U_G) \tag{25}$$

such that the numerical step-by-step scheme becomes second-order-accurate in the mesh size, h.

In a similar procedure, Eqs. (22b) and (23b) applied along the same characteristics b_1 and a_2 of Fig. 2 give two extra equations relating V_G, U_G, and Y. These are also solved to obtain U and V at point G as functions of U, V, and Y at the points A and B, viz.,

$$V_G = 0.5(V_A + V_B) + 0.5Y(U_A - U_B)$$

$$U_G = 0.5(V_A + U_B) + 0.5Y^{-1}(V_A - V_B) \tag{26}$$

In Eqs. (26) Y is also approximated by average values resembling those in Eqs. (25) to maintain a second-order-accurate scheme. Equations (24) and (26) are then solved iteratively for the four unknowns X, Y, U, and V at point G.

Having solved for the four unknowns at all grid nodes, we then proceed to search for points at which the inviscid slip condition

$$(a^* + \bar{u})dr - \bar{v}dx = 0 \tag{27}$$

is satisfied. Equation (27), when expressed in terms of the earlier defined variables X, Y, V, and U, reduces to

$$\lambda(1 + 1.5\lambda U^{2/3})YdY - VdX = 0 \tag{28}$$

with λ being a constant defined by Eq. (6c). It is noteworthy to mention here that Eq. (28) is identically satisfied along any streamline of the flow including the solid surface of the body. It is therefore important to distinguish the zero streamline representing the solid surface of the body from other streamlines of the flow.

Let R represent the magnitude of the residual resulting from applying Eq. (28) between any two points in the supersonic region, i.e.,

$$R = \lambda(1 + 1.5\lambda U^{2/3})YdY - VdX \tag{29}$$

Referring to Fig. 2, since point A lies on the surface of the solid body we apply Eq. (29) between point A and any other point, say N, between points B and G on the b_1 characteristic. The values of U, V, X, and Y at point N are found using linear interpolation from those values at points B and G. If $R>0$, this implies that N is a point away from the surface of the body (i.e., an external point); and if $R=0$ this implies that point N lies on the surface of the body. Here, the exact location of point N at which $R=0$ is found iteratively. The procedure is then repeated. Using point N, we search along BH or HI for a point at which $R=0$, and so forth. Finally, the values of X, Y, and U along the path

representing the locus of points where $R=0$ are utilized in conjunction with Eqs. (5a) and (5b) to determine the shape of the slender body under the sonic bubble, and the supercritical pressure distribution, respectively. It should be mentioned that the slope of the resulting body is always continuous across the sonic line. As we approach point A or F on the sonic line (see Fig. 2), a limiting study of Eqs. (7) and (9) shows that $U\sim t^2$, $Y\sim t^{1/3}$, and $X\sim t^{5/3}$. Therefore, the local slope of the body as we approach either point is given by $dY/dX\sim t^{-4/3}$.

Since $t=0$ along the sonic line, the slopes at points A and F are infinite which indicates that the line $t=0$ is tangent to the body at these two points. It is therefore the singular behavior in $dY(s,0)/dx(s,0)$ at points A and F which guarantees a continuous slope of the body across the sonic line in the physical plane.

Summary and Discussion of Results

In this section a number of slender-body designs are presented, and some experience with the design procedure is discussed. The numerical computations for the inverse and direct problems were performed on a 64×64 mesh with boundary conditions representing the full body. In the lateral direction r, a $t^{2/3}$ mesh stretching was utilized. Since only symmetric bodies (fore and aft) were generated in this study, the results are shown for the bodies truncated at one-half their length. Two examples of slender-body designs having cusped and sharp leading edges are presented in Figs. 3 and 4, respectively. Comparisons with the results obtained from the direct computation of the flowfield utilizing the slender-body designs as input are also illustrated in Figs. 3b and 4b.

For the design of supercritical slender bodies having cusped or sharp leading edges, Figs. 3a and 4a illustrate the different input perturbations U and the unstretched radial coordinates Y required for the design procedure. The resulting slender body shapes and their pressure distributions are given in Figs. 3b and 4b.

Experience has shown that, like the two-dimensional airfoil design problem where constraints are imposed on the input pressure and free-stream Mach number,[25-27] the input function U and the free-stream conditions cannot be prescribed arbitrarily. Conversely, the function Y representing the unstretched radial coordinates of the subsonic portions of the body and its sonic line is arbitrarily prescribed, provided it is consistent with the physics of the flow problem and the boundary conditions for the U boundary value problem. For example, prescribing $Y=g_2(s)$ along the sonic line (cde) while setting $U\neq0$ along that segment implies inconsistency in the boundary conditions for the coupled U-Y boundary value problems, which in turn leads to a nonconvergent solution. It should be emphasized here that this observation does not lead to a mathematically ill-posed problem as may first appear since a complete definition of the body geometry, i.e., $Y(X)$ is not prescribed. Here, we only prescribe the radial coordinate Y and we obtain the amount of axial stretching X as part of the solution. It is also noteworthy to mention here that the familiar body-closure problem[25] does not appear since only flows at zero incidence are considered in this study.

In Figs. 3b and 4b it can be seen that results obtained from the present design procedure and those obtained from the direct computation of the flow past the designed bodies show good agreement. The principal discrepancies, most apparent for the body having a sharp leading edge (Fig. 4b), are confined to the leading edge region. This discrepancy is undoubtedly associated with the logarithmic singularity present in the input perturbation velocity distribution at the leading and trailing edges. Numerical experiments have shown that adjusting the constant A_1 in Eq. (15), to a certain extent, has a direct effect on altering the amount of discrepancy. The slight disagreement between the supercritical pressures that is observed in Figs. 3b and 4b is primarily due to the numerical difficulty in computing the normal derivative $(\partial Y/\partial t)$ in Eq. (17) along the sonic line; this has a direct effect on the sonic line coordinates and consequently on the supercritical pressures. To alleviate this numerical difficulty a $t^{2/3}$ stretching in the mesh was used to capture the singular behavior of $\partial Y/\partial t$ near the sonic line.

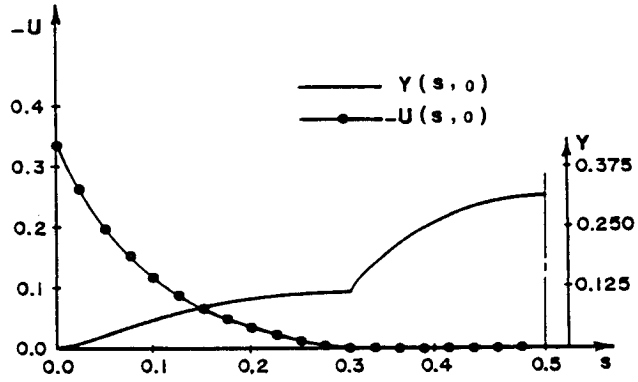

Fig. 3a Input perturbation velocity distribution U, and unstretched radial coordinates Y, for a supercritical symmetrical slender body with cusped leading and trailing edges at $M_\infty=0.843$ and zero incidence.

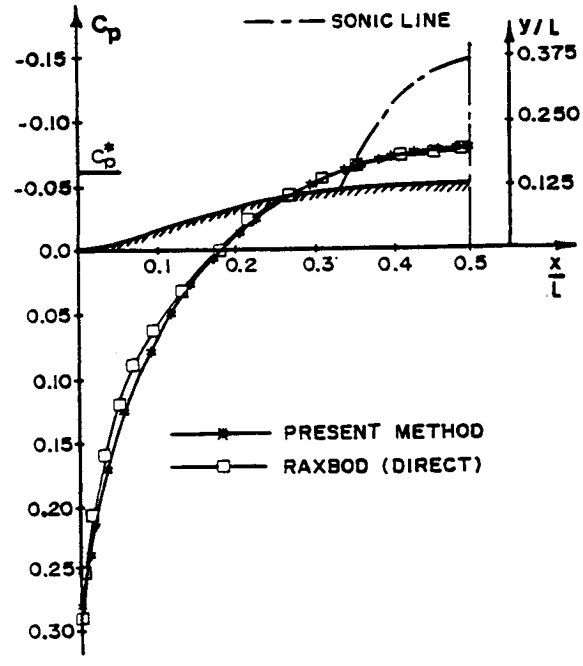

Fig. 3b Pressure distributions and corresponding shock-free supercritical slender body with cusped leading and trailing edges after stretching at $M_\infty=0.843$ and zero incidence.

The far-field boundary in the computational plane $(t=1)$ transforms to a slightly irregular, yet symmetric boundary (about an axis passing through midbody point, i.e., $X/L=0.5$) in the physical plane. For test cases considered here and many others nonreported, the minimum physical distance between the far-field boundary and the resulting body was consistently over 18 body lengths. On the irregular far-field boundary, the flow behavior resembled that in the far field of an axisymmetric dipole. This far-field behavior was first verified by Sobieczky in his solution to Eqs. (9) utilizing hypergeometric functions. Moreover, numerical experiments have shown that increasing or decreasing the constant B_1 in Eq. (11) has a direct effect on decreasing or increasing, respectively, the minimum physical distance between the far-field boundary and the resulting body.

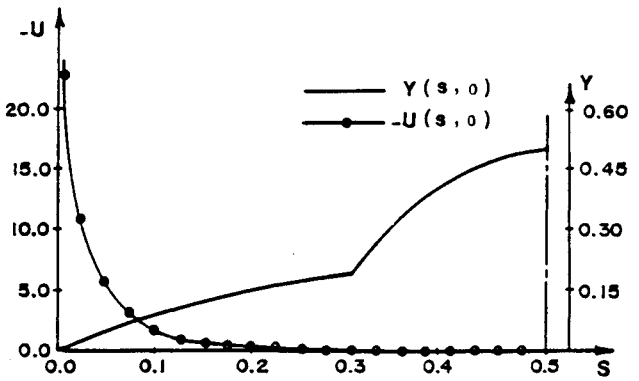

Fig. 4a Input perturbation velocity distribution U, and unstretched radial coordinates Y, for a supercritical symmetrical slender body with sharp leading and trailing edges at $M_\infty = 0.931$ and zero incidence.

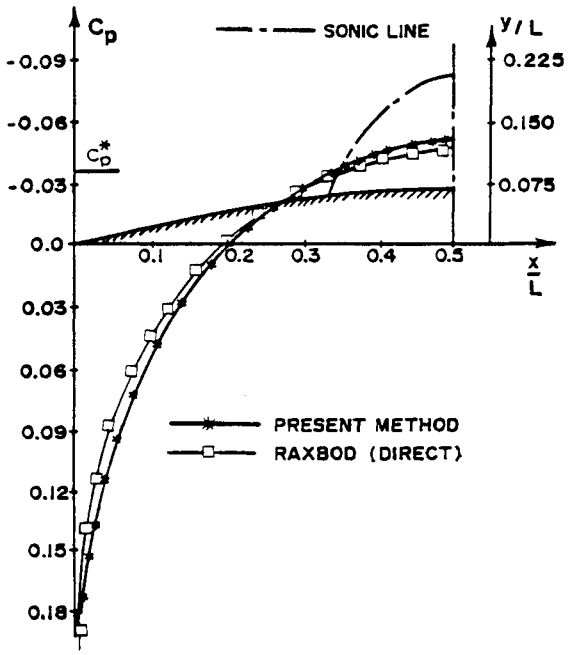

Fig. 4b Pressure distributions and corresponding shock-free supercritical slender body with sharp leading and trailing edges after stretching at $M_\infty = 0.931$ and zero incidence.

Numerical experiments have also shown that including the third and fifth harmonics in the numerical representation of the far-field values for Y in Eq. (13) does not have a noticeable effect on the resulting body of revolution. It was also noticed that special attention must be given to the functional values of $g_2(s)$ in Eq. (16) (representing the unstretched radial coordinates of the sonic line), in relation to the far-field values of Y given by Eq. (13). For example, a value of $g_2(s)$ along the sonic line equal to that of Y on the far-field boundary, line ag in Fig. 2, would physically imply a sonic line touching the far-field boundary. This situation is avoided by adjusting the constant B_2 in Eq. (13).

Numerical experiments also indicate that there seems to be a limitation on the range of free-stream Mach numbers at which shock-free designs are found using the present method. For example, at $M_\infty = 0.94$ a symmetrical fore and aft body was generated using the present procedure. When this body geometry was utilized as input to the direct computation using RAXBOD, it was noticed that a shockwave existed at approximately $X/L = 0.86$ with a very clear asymmetry in the computed pressure distribution. Attempts to remove the shock were made by altering the shape of the unmapped sonic line $g_2(s)$, as it might represent an inconsistency with shock-free flow at $M_\infty = 0.94$, but with no success. In this attempt, we were primarily motivated by our experience with limit lines in the hodograph plane as their presence signaled an inconsistency between the input shape of the sonic line, the free-stream Mach number, and the resulting airfoil section. Further attempts to remove the shock included altering the constants B_1, B_2, A_1, and A_2 in Eqs. (11, 13, 15) but with no further success. This test case and a number of others at higher Mach number will be discussed in a future publication.

Conclusion

It has been demonstrated here that a design procedure resembling that for two-dimensional subcritical and supercritical airfoils (Hassan[28]) can be applied to design shock-free slender bodies of revolution. As in the case of two-dimensional flows, the results are shown, by comparison with other numerical results, to have a good accuracy considering both the small perturbation and slender-body approximations inherent in the fundamental equations.

The results of this investigation are of interest, not only because of the frequent use of a body of revolution in aeronautical design, but also because of the central role of the body of revolution in applications of the transonic area and equivalence rules. Moreover, while the results are given for inviscid flow, the same procedure can be employed iteratively with a boundary-layer calculation in order to achieve viscous slender body designs. For supercritical bodies, the shock-free pressure field should make the boundary-layer calculation reliable. Though the method seems to be reliable in generating shockless bodies at free-stream Mach numbers less than 0.931, caution should be practiced at higher Mach numbers as the method produces bodies which are inconsistent with shock-free flow. Unfortunately, like most design methods, the need for choosing appropriate input constants to approach a given target pressure distribution remains one of the major shortcomings of this method. As previous discussions have indicated, successive trials in most cases quickly indicate suitable values for these constants. A more systematic method, probably involving numerical optimization, would greatly enhance the effectiveness of this method.

Finally, the computational efficiency and cost effectiveness of the design procedure are evident. Computation time is 30-40 CPU s on an IBM 370 for subcritical designs and 60-75 CPU s for shock-free supercritical designs.

Acknowledgment

I would like to thank Professor H. Sobieczky who suggested this research topic and Professor A. R. Seebass who in many respects made this work possible.

References

[1]Hayes, W. D., "Linearized Supersonic Flow," Ph.D. Dissertation, California Institute of Technology, Pasadena, CA, 1947.

[2]Whitcomb, R. T., "A Study of the Zero-Lift Drag-Rise Characteristics of Wing-Body Combinations Near the Speed of Sound," NACA Rept. 1273, 1956.

[3]Oswatitsch, K. and Kuene, F., "Ein Äquivalensatz für nichtangestellte Flügel kleiner Spannweite in Schallnäher Strömung. Zeitschrift für Flugwissenschaften," 3 Jahrgang, Heft 2, S.29, 1955.

[4]Lomax, H., "The Wave Drag of Arbitrary Configurations in Linearized Supersonic Flow as Determined by Areas and Forces in Oblique Planes," NACA RM A55A18, 1955.

[5]Dalton, C. and Zedan, M. F., "Design of Low Drag Axisymmetric Shapes by the Inverse Method," ASME Book Number G00147, New York, 1979.

[6]Stratford, B. S., "The Prediction of Separation of the Turbulent Boundary Layer," *Journal of Fluid Mechanics*, Vol. 5, No. 1, 1959.

[7]Keune, F. and Oswatitsch, K., "On the Influence of the Geometry of Slender Bodies of Revolution and Delta Wings on

Their Drag and Pressure Distribution at Transonic Speeds," KTH-Aero TN42, 1956.

[8]Kusukawa, K., "On the Transonic Flow of A Compressible Fluid Past an Axisymmetric Slender Body at Zero Incidence," *Journal of Physical Society of Japan*, Vol. 12, 1957, p. 401.

[9]Spreiter, J. and Alksne, A., "Aerodynamics of Wings and Bodies at Mach Number One," *Proceedings of the Third U.S. National Congress of Applied Mechanics*, 1958, pp. 27.

[10]Spreiter, J. and Alksne, A., "Slender-Body Theory Based on Approximate Solution of the Transonic Flow Equation," NASA TR-R2, 1959.

[11]Krupp, J. and Murman, E., "Computation of Transonic Flows Past Lifting Airfoils and Slender Bodies," AIAA Paper 71-566, 1971.

[12]Sedin, C. J., "Axisymmetric Sonic Flow Computed by a Numerical Method Applied to Slender Bodies," AIAA Paper 74-544, 1974.

[13]Zannetti, L., "A Time-Dependent Method to Solve the Inverse Problem for Internal Flows," AIAA Paper 79-0013, 1979.

[14]Nelson, D., Hudson, G., and Yang, T., "The Design Performance of Axially Symmetrical Contoured Wall Diffusers Employing Suction Boundary Layer Control," ASME Paper 74-FT-152, 1974.

[15]Shankar, V., "Numerical Boundary Condition Procedure for the Transonic Axisymmetric Inverse Problem," NASA Conference Publication No. 2201, 1981, p. 183.

[16]Hicks, R. and Vanderplaats, G., "Application of Numerical Optimization to the Design of Supercritical Airfoils without Drag Creep," Society of Automotive Engineers Paper 770440, 1977.

[17]Hicks, R. and Henne, P., "Wing Design by Numerical Optimization," AIAA Paper 77-1247, 1977.

[18]Chan, Y. and Mundie, D., "Transonic Axisymmetric Bodies with Minimal Wave Drag," *Canadian Aeronautics and Space Journal*, Vol. 26, 1980, p. 231.

[19]Miele, A., "Theory of Optimum Aerodynamic Shapes," Academic Press, New York, London, 1965.

[20]Malmuth, N. D., Wu, C. C., and Cole, J. D., "Slender Body Theory and Optimization Procedures for Transonic Wing-Bodies," AIAA Paper 83-0184, 1983.

[21]Sobieczky, H., "Transonic Fluid Dynamics Lecture Notes," College of Engineering, The University of Arizona, Rept. TFD 77-01, 1977.

[22]RAXBOD, "A Fortran Program for Inviscid Transonic Flow over Axisymmetric Bodies," Technololgy Utilization Office, NASA Langley Research Center Rept. LAR-12499, 1976.

[23]Ashley, H. and Landahl, M., *Aerodynamics of Wings and Bodies*, Addison-Wesley Publishing Company, Inc., 1965.

[24]Sweet, R. A., "Direct Methods for the Solution of Poisson's Equation on a Staggered Grid," *Journal of Computational Physics*, Vol. 12, 1973, p. 422.

[25]Lighthill, M. J., "A New Method of Two-Dimensional Aerodynamic Design," Aeronautical Research Council, R&M 2112, London, England, 1945.

[26]Volpe, G. and Melnik, R. E., "The Role of Constraints in the Inverse Design Problem for Transonic Airfoils," AIAA Paper 81-1233, 1981.

[27]Hassan, A. A., Sobieczky, H., and Seebass, A. R., "Transonic Airfoils with a Given Pressure Distribution," AIAA Paper 81-1235, 1981.

[28]Hassan, A. A., "Subcritical and Supercritical Airfoils for a Given Pressure Distribution," Ph.D. Dissertation, University of Arizona, 1981.